Journal of Materials Chemistry B

ROYAL SOCIETY OF CHEMISTRY

PAPER

View Article Online
View Journal | View Issue

Cite this: J. Mater. Chem. B, 2024, 12, 5699

Rationally designed protein A surface molecularly imprinted magnetic nanoparticles for the capture and detection of *Staphylococcus aureus*†

Kritika Narula,[a] Soumya Rajpal,[a] Snehasis Bhakta,[b] Senthilguru Kulanthaivel[a] and Prashant Mishra *[a]

Staphylococcus aureus (*S. aureus*), a commensal organism found on the human skin, is commonly associated with nosocomial infections and exhibits virulence mediated by toxins and resistance to antibiotics. The global threat of antibiotic resistance has necessitated antimicrobial stewardship to improve the safe and appropriate use of antimicrobials; hence, there is an urgent demand for the advanced, cost-effective, and rapid detection of specific bacteria. In this regard, we aimed to selectively detect *S. aureus* using surface molecularly imprinted magnetic nanoparticles templated with a well-known biomarker protein A, specific to *S. aureus*. Herein, a highly selective surface molecularly imprinted polymeric thin layer was created on ~250 nm magnetic nanoparticles (MNPs) through the immobilization of protein A to aldehyde functionalized MNPs, followed by monomer polymerization and template washing. This study employs the rational selection of monomers based on their computationally predicted binding affinity to protein A at multiple surface residues. The resulting MIPs from rationally selected monomer combinations demonstrated an imprinting factor as high as ~5. Selectivity studies revealed MIPs with four-fold higher binding capacity (BC) to protein A than other non-target proteins, such as lysozyme and serum albumin. In addition, it showed significant binding to *S. aureus*, whereas negligible binding to other non-specific Gram-negative, *i.e. Escherichia coli* (*E. coli*), *Pseudomonas aeruginosa* (*P. aeruginosa*), and Gram-positive, *i.e. Bacillus subtilis* (*B. subtilis*), bacteria. This MIP was employed for the capture and specific detection of fluorescently labeled *S. aureus*. Quantitative detection was performed using a conventional plate counting technique in a linear detection range of 10^1–10^7 bacterial cells. Remarkably, the MIPs also exhibited approximately 100% cell recovery from milk samples spiked with *S. aureus* (10^6 CFU mL^{-1}), underscoring its potential as a robust tool for sensitive and accurate bacterial detection in dairy products. The developed MIP exhibiting high affinity and selective binding to protein A finds its potential applications in the magnetic capture and selective detection of protein A as well as *S. aureus* infections and contaminations.

Received 24th February 2024,
Accepted 3rd May 2024

DOI: 10.1039/d4tb00392f

rsc.li/materials-b

1. Introduction

S. aureus is a commensal bacteria that colonises the human skin and is known to cause infections of the skin, pneumonia, bacteremia and infective endocarditis.[1] *S. aureus* is also a typical food-borne, zoonotic and nosocomial pathogen[2] that expresses an array of extracellular toxins and enzymes that help in its virulence.[3] Its isolates have shown resistance to antibiotics such as methicillin and, in some cases, carbapenems and vancomycin; hence it is a threat to both human health and animal husbandry.[4]

Current gold standard tests for detecting *S. aureus* are culture based and rely on enrichment and separation on selective plates, biochemical tests and 16S rRNA sequencing.[5,6] Although this approach is simple, it is typically time consuming as the process takes 4–7 days.[7] In view of this, various rapid detection methods, such as ELISA,[8] PCR,[9] loop-mediated isothermal amplification,[10] and fluorescence-based methods,[11] have been developed to reduce assay time. PCR is a relatively quick method but may give false positives owing to the mispairing of primers and requires expensive equipment.[12] Antibody-based tests such as ELISA are rapid but suffer from high cost, and low stability of antibodies. Hence, there is an urgent requirement for a selective, sensitive, cost-effective and

[a] Department of Biochemical Engineering and Biotechnology, Indian Institute of Technology Delhi, New Delhi, India. E-mail: pmishra@dbeb.iitd.ac.in
[b] Department of Chemistry, Cooch Behar College, West Bengal, India

† Electronic supplementary information (ESI) available. See DOI: https://doi.org/10.1039/d4tb00392f

stable method for the rapid detection of *S. aureus* from various sources. Protein A is a characteristic component of the *S. aureus* cell wall that binds to the Fc component of IgG antibodies and plays a critical role in defence against the host immune system. Owing to its high expression and location on the cell surface, protein A has great potential to be used as a biomarker for the specific recognition of *S. aureus*.

Molecularly imprinted polymers (MIPs) generally considered artificial antibodies or synthetic receptors have structure predictability, recognition specificity, and application universality.[13,14] Unlike antibodies, MIPs are more stable, economical, and easy to synthesize. Earlier, protein A-imprinted polyacrylamide gel beads were synthesized using inverse suspension polymerization and bulk polymerization to detect protein A and *S aureus*. Bulk polymerization-based MIPs have shown an adsorption capacity of 10^3–10^4 colony-forming unit (CFU) g^{-1} gel beads.[15,16]

Recently, *S. aureus* whole cell imprinted polymer and turn on fluorescence probe have been synthesized for the detection of the organism.[17,18] Although bulk imprinting of polymers has shown potential for small molecules, it has limited applications for larger molecules, such as proteins. Nonetheless, surface imprinting involves the restriction of a target molecule's binding site only to the surface of a nanomaterial[19–23] and hence suitable for binding larger molecules, such as proteins or a whole bacterial cell. In addition, it requires fewer template molecules for imprinting and shows better selectivity, fast absorption rates, and good synthesis reproducibility.[24] Further, it is prudent to enhance the translation potential of the MIP technology to the industrial scale, which is limited due to its reproducible nature and comparable high specificity of antibodies. With the intervention of *in silico* design, it is possible to design MIPs with optimal potential.[13,25–27]

Computational tools offer a more efficient and cost-effective screening of potential monomers for MIP synthesis. By simulating interactions between monomers and the target protein, we can rationally select candidates based on their binding affinity and specificity, thereby reducing the need for extensive experimental testing. Among various computational tools, molecular docking offers the estimation of monomer binding affinity with a target protein of interest with significant improvement in MIP development because it directly mimics the pre-polymerization reaction mixture.[28,29] The arrangement, orientation, and interaction through ionic, hydrophobic, and hydrogen bonding of monomers at multiple (surface) residues of the protein can be predicted to essentially improve the recognition ability of MIPs.

In the present work, based on computationally guided design, protein A-binding surface imprinted magnetic nanoparticles were synthesized for the specific detection of *S aureus.* A set of protein-compatible monomers commonly employed for molecular imprinting were screened using molecular docking to protein A. Based on the binding energy (kcal mol^{-1}) values and multi-point interaction analysis, high-performing monomers were selected and employed in various combinations to design target-specific imprinted layers. Unlike previous studies that used a single monomer with limited types of molecular interactions with the target, this study involves multiple types of interactions (ionic interactions, hydrogen bonding, van der Waals forces and π–π interactions), which are deployed using a multi-monomer approach, leading to optimal binding ability.[30]

Core–shell surface imprinting was applied for the first time for *S. aureus* detection. Herein, protein A was used as a template for the effective construction of an imprinted ''shell'' on a magnetite nanoparticle (Fe_3O_4) ''core''. The magnetite nanoparticles synthesized were spherical and possessed a diameter of approximately 250 nm. Polymerization was performed on the surface according to the selected monomer composition. Molecular docking revealed dopamine as the best binding monomer in terms of binding energy and silane monomers in terms of improved multi-point interactions. However, the experimental analysis demonstrated silane-based MIPs with a high BC of ∼11 mg g^{-1} and an imprinting factor of ∼ 5, establishing the importance of interaction with multiple surface residues. In addition, MIP bonded to the *S. aureus* in a broad linear range of 10^1–10^7 CFU mg^{-1}. Furthermore, at least four-fold higher binding of MIP to protein A than non-target proteins was demonstrated. Hence, synthesized MIP nanoparticles can be utilized to capture and detect *S. aureus*, leading to their potential applications in healthcare and the food industry.[31]

2. Experimental section

2.1. Chemicals

Tetraethoxysilane (TEOS), (3-aminopropyl) triethoxysilane (APTES), phenyltriethoxysilane (PTES), ureidopropyltrimethoxysilane (UPTMS), ferric chloride hexahydrate ($FeCl_3{\cdot}6H_2O$), NH_4OH (25% ammonium hydroxide aqueous solution), glutaraldehyde (25% aqueous solution), polyethylene glycol 2000, ammonium persulfate (APS), dopamine (DA), sodium acetate (NaAc), protein A, human serum albumin (HSA) and lysozyme were purchased from Sigma-Aldrich. Absolute ethanol was procured from Merck. A Quick Start Bradford protein assay kit was obtained from Bio-Rad.

2.2. Characterization techniques

The nanoparticle size and morphology were determined using high-resolution transmission electron microscopy (HRTEM) Tecnai G2 20. The magnetic properties of the nanoparticles were investigated using PPMS from Cryogenic Limited, UK. Zeta potential measurements were performed using the Zeta Malvern Zetasizer Nano-ZS90. Surface functional groups were investigated using a Fourier-transform infrared (FTIR) spectrophotometer from Thermo Scientific Nicolet iS50 with ATR mode. UV-visible spectra were obtained using an Eppendorf BioSpectrometer. The X-ray diffraction (XRD) pattern was taken using an X-ray diffractometer from Rigaku Ultima IV, energy-dispersive X-ray (EDAX). Hitachi TM3000 was used for the elemental composition. Fluorescence studies were executed using a Zeiss Axio Observer inverted microscope. Ultrasonication was

performed using Branson model 2800. Particles were freeze dried using Allied Frost Lyophilizer-FD-3.

2.3. Synthesis of magnetic nanoparticles

Fe_3O_4 nanoparticles were synthesized using the solvothermal method.[32] Briefly, $FeCl_3{\cdot}6H_2O$ (1.35 g), NaAc (3.6 g), and polyethylene glycol (1.0 g) were dissolved in ethylene glycol (40 mL). The mixture was stirred for 30 min. It was then sealed in a Teflon-lined stainless-steel autoclave vessel and kept for 16 h at 200 °C. The product was washed three times with ethanol and water. The particles were then freeze-dried under a vacuum.

2.4. Surface modification of Fe_3O_4 particles

Silica coating was done to improve the stability of the magnetic core and facilitate surface functionalization.[33,34] In brief, 100 mg of Fe_3O_4 nanoparticles were dispersed in 20 mL ethanol and 3 mL MiliQ water (resistivity of 18.2 MΩ cm^{-1}). The above solution was treated with 1 mL of 25% ammonia aqueous solution under stirring at 40 °C. Then, 0.2 mL of TEOS was added to the mixture and stirred for 5 h, at room temperature (RT). Silica-coated magnetic nanoparticles (Fe_3O_4@SiO_2) were captured by applying an external magnetic field, which was then washed three times and freeze-dried under a vacuum.

2.5. Functionalization of Fe_3O_4 nanoparticles

Silica-coated magnetic nanoparticles were sequentially functionalized with APTES and glutaraldehyde to generate an aldehyde group on the surface of the nanoparticles for protein immobilization.[35] To make a 3.0 mg mL^{-1} Fe_3O_4@SiO_2 solution, 60 mg nanoparticles were dispersed in 20 mL of 10 mM phosphate buffer (PB), with a pH of 7.3. Then, in a round bottom flask, 22 μL of APTES was added to 20 mL of nanoparticle solution and kept under continuous stirring (400 rpm) for 2 h at RT. This was followed by washing the nanoparticles with MilliQ water. To obtain aldehyde-functionalized nanoparticles, 20 mL of amine-functionalized nanoparticles were resuspended in 1% (v/v) aqueous glutaraldehyde solution and stirred for 20 minutes at RT. These functionalized nanoparticles were washed multiple times and resuspended in PB (pH 7.4).[36,37]

2.6. Computational methods

The structural files for all monomers were obtained from the PubChem databank (Fig. S1, ESI†). The crystal structure of the monomer unit of protein A was extracted from PDB ID:1DEE using the UCSF Chimera.[38] For molecular docking, Autodock 4.2.6 based on the AMBER force field was employed.[39] The monomer files were converted to a pdbqt format after setting the torsional degrees of freedom based on the detected rotatable bonds. Using Autodock tools, polar hydrogens were added to the protein, and water molecules were deleted. A grid box with dimensions of 114 × 76 × 98 Å was centred on the protein. The estimated monomer-binding energy to the protein is represented as kcal mol^{-1}. The mean binding energy of the first rank in the clustering histogram was used to compare the monomers for their high binding affinity. The remaining conformational clusters were employed to visualize all possible binding poses in the root mean square deviation (RMSD) tolerance set at 2 Å. This enables the analysis of favourable multi-point interactions on the surface of the protein consisting of hydrogen bonds, electrostatic interactions, and van der Waals interactions.

Table 1 Amount of monomers and cross-linkers for MIP synthesis

Monomers	Dopamine	APS[a]	TEOS[b]	APTES	PTES	UPTMS
Set 1	12 mg	1.2 mg	—	—	—	—
Set 2	—	—	1 mg	—	—	—
Set 3	—	—	1 mg	1 mg	—	—
Set 4	—	—	1.2 mg	0.26 mg	0.26 mg	0.26 mg

[a] APS is the initiator for dopamine polymerization. [b] TEOS is cross-linkers for silane monomers.

2.7. Molecularly imprinted polymer (MIP) synthesis

Initially, to immobilize the protein molecules onto the nanoparticle surface, 18 μg protein A was added to 1 mL of 3 mg mL^{-1} aldehyde-functionalized nanoparticle solution and stirred for 3 hours. Protein A immobilized nanoparticles were resuspended in 1 mL of PB, with pH 7.3 containing different monomer amounts, as presented in Table 1. The polymerization reaction was allowed to take place for 16 h at RT on a 360° rotator, as reported.[40,41] Polymerized nanoparticles were washed several times using methanol and acetic acid (9 : 1) solution to remove the bound template[42] (Fig. 1). Non-imprinted polymer (NIP) was synthesized following the exact procedure of MIP synthesis, except for the protein A addition step.

2.8. Binding studies

To select the monomer combination for MIP synthesis, different combinations of monomers, as presented in Table 1, were evaluated owing to their protein binding properties. A batch experiment was performed in which 0.25 mg of MIP of each combination was suspended in 0.5 mL of 20 μg mL^{-1} protein A solution in PB (10 mM, pH 7.2). The mixture was then incubated for 2 h under slow rotation on a 360° rotator at RT. The supernatant was collected using magnetic separation, and the concentration of protein A in the unbound fraction was determined using the Bradford assay.[43] The equilibrium adsorption amount or BC (q, mg g^{-1}) was calculated to bind MIP, and NIP to protein A, using eqn (i):

$$q = (C_i - C_f)V/m, \quad \text{(i)}$$

where C_i and C_f are the initial and final concentrations (mg mL^{-1}) of protein A in the solution, respectively; m is the amount of MIP (g); and V is the volume of protein A solution (mL).[44,45]

The imprinting factor was determined using eqn (ii):

$$IF = q_{MIP}/q_{NIP}, \quad \text{(ii)}$$

where IF is the imprinting factor and q_{MIP} and q_{NIP} are the adsorption amount of the MIP and NIP, respectively.

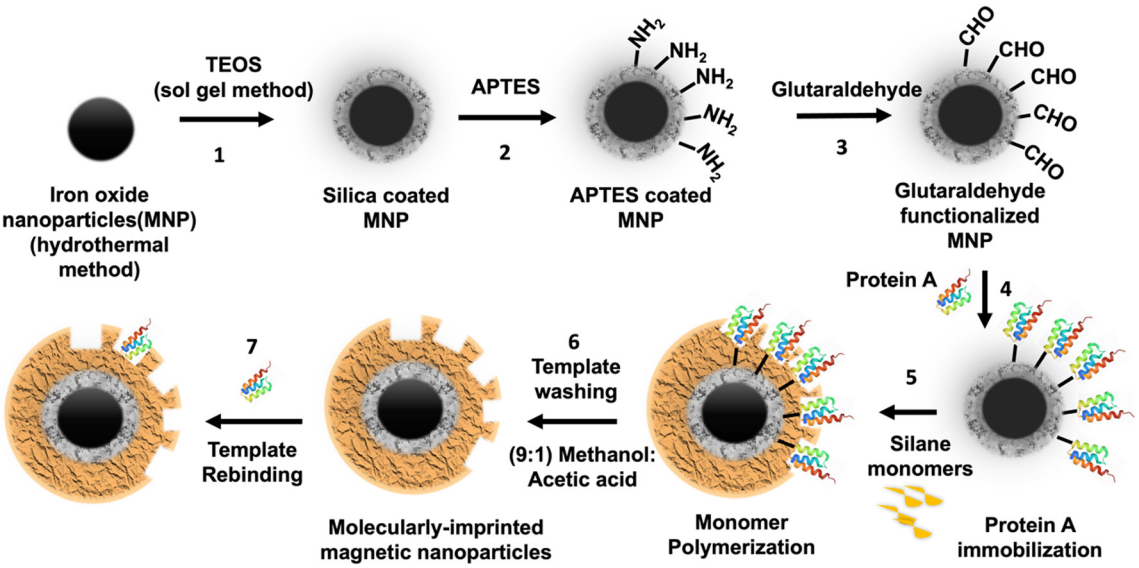

Fig. 1 Schematic illustration of the surface imprinting process to generate a 'core–shell' type imprinted polymer on magnetic nanoparticles for specific binding to protein A. (1) Hydrothermally synthesized iron oxide nanoparticles treated with TEOS for silica coating, (2) followed by APTES treatment to generate amine group on the surface. (3) Modification using 1% glutaraldehyde to add surface aldehyde groups. (4) Protein A immobilization by imine bond formation between free amine groups of protein and aldehyde groups on the surface of nanoparticles. (5) MIP synthesis using suitable monomer combinations. (6) Protein removal using methanol : acetic acid (9 : 1) to create cavities complementary to the size and shape of the template. (7) Protein A rebinding to evaluate MIP BC.

To investigate the selectivity, BC of MIP with non-specific proteins, such as HSA, BSA, and Lysozyme, was determined. 0.35 μM of non-specific proteins were added to 0.5 mg mL^{-1} of MIP and NIP each. The BC was determined as described above.

To determine the binding properties of the selected MIP, a batch experiment involving 0.25 mg of MIP and NIP each was suspended in 0.5 mL of a protein A solution in PB buffer, (10 mM, pH 7.2) at a varying concentration range of 0–40 μg mL^{-1}. BC was determined at different protein A concentrations, and the binding isotherm was plotted.

2.9. Bacterial binding studies

To evaluate the binding characteristics of the MIP with the target bacteria, a batch experiment was conducted in which 1 mg MIP was added in 10 mL Phosphate Buffered Saline (PBS) at pH 7.4 containing 10^1–10^7 CFU mL^{-1} *S. aureus.* The suspensions were kept in a shaker for 2 h at RT. The concentration of *S. aureus* bound to the MIP was determined by plating the unbound bacteria left in a supernatant after treatment with MIP (subtraction method). BC was determined at various bacterial concentrations, and a binding isotherm was plotted for MIP.

To evaluate the selectivity of MIP against bacteria, binding studies with *S. aureus*, *B. subtilis*, and *E. coli* were performed and visualized using fluorescence microscopy. For this purpose, the bacteria were pre-stained with acridine orange. For staining, bacterial cells (10^7 CFU mL^{-1}) were resuspended in PBS (pH 7.4) containing 100 μg mL^{-1} acridine orange. The suspension was incubated for 30 min at 37 °C. The excess stain was removed by washing the cells three times with PBS. Next, 200 μg of MIP was added to the 1 mL stained bacterial cells. The solution was allowed to rotate at RT for 2 h on a 360° rotator. The unbound bacteria were removed by washing with PBS three times, and the MIP was resuspended in 20 μl PBS. Finally, the sample was placed on a glass slide and visualized using a fluorescence microscope.

2.10. *S. aureus* detection in real samples

The validation and assessment of the MIP's applicability depend on the analysis of real samples. To conduct real sample experiments, milk samples were spiked with *S. aureus*. Specifically, *S. aureus* was added at a concentration of 10^6 CFU mL^{-1} to a milk sample diluted ten-fold with PBS at pH 7.4. Following a 2-hour incubation period with MIP and NIP, magnetic separation was done to capture MIP-bound bacteria. The unbound fraction was subsequently plated for cell counting. This approach allowed for a comprehensive evaluation of the MIP's performance using real samples.[46]

3. Results and discussion

3.1. Computational screening of functional monomers

The nature's design of the antigen–antibody complex formation, involving a unique set of interactions at multiple amino acid residues to form a specific lock-key complex, can be mimicked using molecular imprinting technology. The polymeric cavity can be tailored to project functional groups that enable complementary binding to the target analyte. Herein, *S. aureus* specific biomarker, protein A, with negative surface charge at pH 7.0 and predominated hydrophilicity[47] is selected as a template for MIP. Protein A exists in both secretory and membrane-bound forms, thereby allowing both direct and indirect bacterial identification.

Table 2 Screening of functional monomers for optimal binding with protein A using Autodock 4. The docked monomers are ranked (I–X) in the ascending order of estimated binding energy (kcal mol^{-1}). Higher negative values indicate better binding affinity

Rank	Monomers	Estimated binding energy (kcal mol^{-1})	Number of distinct conformational clusters	Number of multi point interactions
I	Dopamine	−4.64	5	4
II	Methacrylic acid (MAA)	−3.81	2	1
III	Phenyltriethoxysilane (PTES)	−3.73	10	4
IV	3-Ureidopropyltrimethoxysilane (UPTMS)	−3.30	9	8
V	*N*-Isopropylacrylamide (NIPAM)	−3.16	6	4
VI	Methacrylamide (mACR)	−3.07	5	4
VII	Aminophenyl boronic acid (APBA)	−3.03	7	4
VIII	Tetraethoxysilane (TEOS)	−2.85	7	5
IX	Acrylamide (ACR)	−2.78	5	4
X	3-Aminopropyltriethoxysilane (APTES)	−2.77	9	6

The crucial step in identifying suitable functional monomers is enabled by a molecular mechanics approach where the whole protein is docked with monomers, and the intermolecular interactions are modelled. The use of monomers that can form multiple non-covalent bonds spanning the entire protein surface with comparatively higher binding energy is likely to result in an enhanced specificity of the MIP. For this, we screened a list of commonly used monomers (for protein A imprinting) to estimate their binding affinity (Table 2). Dopamine with its unique set of functional groups that enables both hydrophobic interactions (phenyl ring) and hydrophilic/ionic interactions (Table 2(I)) produced the strongest binding affinity with protein A (−4.64 kcal mol^{-1}). Additionally, other monomers possessing phenyl rings (Table 2(III; VII)) have higher binding energy due to their ability to form strong π–π interactions with aromatic amino acids. However, the lowest binding affinity was found for the commonly used silane monomer, APTES (−2.77 kcal mol^{-1}), and, therefore, ranked last in the group (Table 2(X)). Visualization and analysis of other distinct conformational clusters of the monomers helped to assess a network of non-covalent interactions on the entire template surface rather than just single-point binding analysis (Fig. 2). These clusters were considered only within a short range of 2 Å distance between the monomer heavy atom and amino acid to account for fairly strong interactions. The largest number of multi-point interactions was observed with each of the silane monomers, mainly UPTMS, and APTES (Table 2(IV, X)), hence validating the increased use of silanes for protein imprinting.[37] The contrasting behaviour of the methacrylic acid monomer yields a higher affinity one-point interaction, but the least number of multiple interactions on the protein surface (two confirmational clusters located at the same point) precisely elaborates this analysis (Fig. 2(II)).

Additionally, the highest ranking dopamine had lesser binding points (4) compared to the lowest-ranking APTES (6) (Table 2). PTES (Table 2(III)) was introduced as one of the monomers to cover hydrophobic regions on the protein surface. TEOS (Table 2(VIII)) is generally used as a crosslinker for silane monomers. *In silico* prediction shows wide range interactions (hydrogen bond, hydrophobic, and electrostatic) between these monomers (Fig. 2(III), (IV), (VIII) and (X)) and protein A, giving further validation for the use of a multi monomer approach for optimal binding efficiency (Fig. S2, ESI†). Overall, this predictive estimation motivated the selection of silane-based monomers (Fig. 2(III), (IV), (VIII) and (X)) for imprinting the target protein A. Simultaneously, we also selected three more combinations: first involves only dopamine, being the highest ranked monomer; second involves APTES and TEOS, which are the lower ranked; and third involves only TEOS as a control polymer to determine the change in BC upon the addition of other silane monomers. Simultaneously, the need for the cross-linker

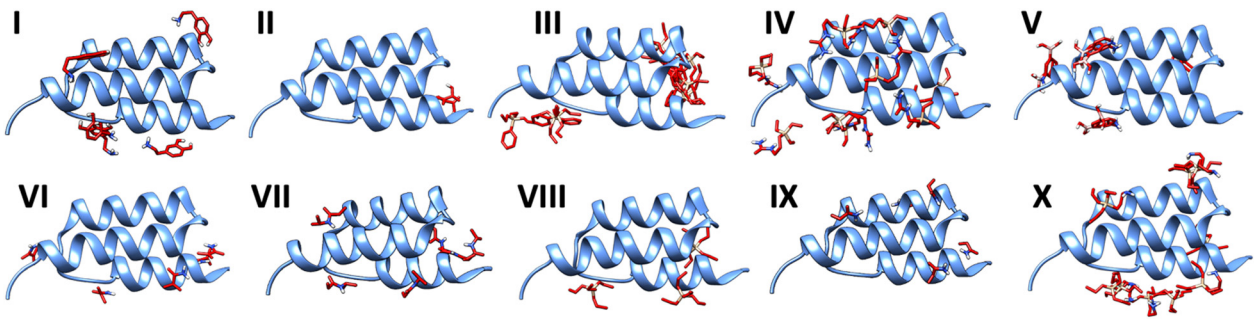

Fig. 2 Visualization of binding poses of monomers (red) clustered on protein A (blue, helical structure). Distinct conformational clusters within RMSD-tolerance of 2 Å are represented for each monomer: I: dopamine, II: MAA, III: PTES, IV: UPTMS, V: APBA, VI: mACR, VII: NIPAM, VIII: ACR, IX: APTES, and X: TEOS. The highest number of multi-point interactions over the entire protein surface are shown in the case of PTES (III), UPTMS (IV), and APTES (IX) and least by MAA (II).

is addressed in each set, as dopamine and TEOS serve as cross-linkers.

Interestingly, the third set utilizing APTES as a positively charged monomer, which interacts with the negatively charged protein A, may offer valuable insights into the effective design of MIPs.

3.2. Experimental design for protein A specific MIPs

In this study, MIPs are innovatively developed as a 'shell' over a magnetic (Fe_3O_4) core offering great utility in terms of easy isolation, specific detection, and reusable nature. In addition, magnetic separation plays a major role in the enrichment of bacteria from large sample volumes, consequently increasing the sensitivity of the method.[48] With the help of molecular imprinting onto magnetic nanoparticles, this can be achieved in a cost-effective and efficient manner. Protein A is a 42 kDa protein that is templated over these core–shell particles with an approximate size of 250 nm. For the magnetic core, Fe_3O_4 nanoparticles were synthesized using the solvothermal method. Further, nanoparticles were functionalized with a silica layer using the sol–gel method with TEOS treatment. This coating provided nanoparticles with chemical stability and prevented aggregation in the solution. Next, hydroxyl groups of SiO_2 on the surface reacted with ethoxy groups of APTES to give the surface the amine group. Then, these amine groups reacted with glutaraldehyde to produce aldehyde-modified Fe_3O_4@SiO_2 nanoparticles.[36] Glutaraldehyde coating is an important step because it helps to immobilize protein A using a Schiff base reaction between an aldehyde and amino groups of the protein. Finally, for imprinting, four sets of monomer combinations as selected from the computational screening were used to synthesize MIPs under constant physical conditions (RT, pH 7.0). In the first set, dopamine was used as a monomer with various advantages, such as high water solubility, polymerization ability under RT, and several amino acid-like functional groups that interact with peptide chains. Dopamine with the highest binding energy at the lowest ΔG value (−4.64) was selected as the monomer for MIP 1. In addition, dopamine demonstrated high BC (8.14) due to the presence of several amino acid-like functionalities present in the structure. The phenyl group, hydroxyl group, free amine group and the ethyl moieties present in the dopamine molecules help to interact with the target biological molecules in a similar fashion present in natural biomolecular interactions. Phenyl groups offering π–π interactions, amines, and hydroxyl groups can help in the formation of hydrogen bonding and ionic interactions, and the ethyl and phenyl groups help to bind *via* hydrophobic interactions. Overall, it is found from computational studies that dopamine is a suitable monomer for protein imprinting; however, non-specific interactions could lead to poor imprinting factors (0.82) due to comparable binding with NIP as well[49] (Fig. 3).

In the next sets, silane monomers with relatively less reactivity under various conditions (*e.g.*, strong acids, bases, and oxidizers) were used; therefore, efficient binding sites are formed due to stable and highly crosslinked silica polymers. Various studies have reported MIPs synthesized using silane monomer combinations and achieved a high IF of 5, which was further increased to 15 *via* cladding using TEOS.[50–53] Furthermore, organosilica hybrid materials can be easily made using molecular precursors that can participate in the hydrolysis and condensation reactions as the metal alkoxide (Scheme 1), which is a flexible way to adjust the MIP's selectivity by choosing the most appropriate functional groups to interact with the template.[54] In addition, these monomers involve polymerization in the aqueous environment, which can facilitate the structural preservation of protein molecules during the process of polymerization, thereby ensuring the optimal rebinding of protein targets.

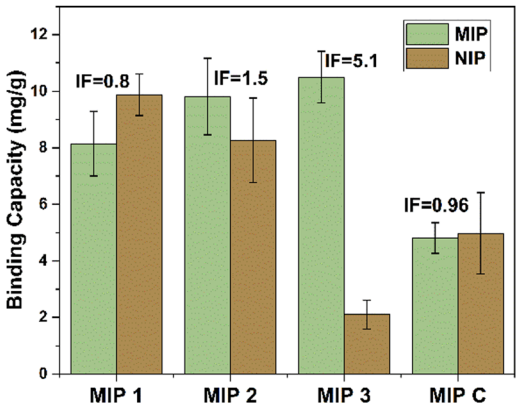

Fig. 3 Binding capacity values for different MIP combinations. Each set of MIP is made using a unique combination of monomers, *i.e.*, MIP 1: dopamine, MIP 2: TEOS and APTES, MIP 3: TEOS, APTES, PTES, UPTMS, and control MIP *i.e.*, MIP C: TEOS. The combination of all four silane monomers (MIP 3) resulted in better binding capacity and imprinting factor. Error bars indicate standard deviation.

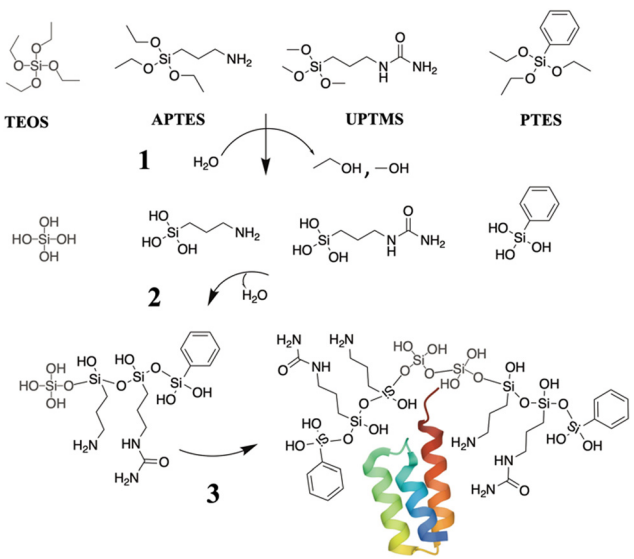

Scheme 1 Co-polymerization pathway of organo-silane monomers used in the molecular imprinting of protein A. (1) Hydrolysis of monomers (2) condensation reaction (3) copolymerization step leading to the formation of specific binding pocket *via* diverse functional groups of siloxane monomers for protein A binding.

Here, for the computationally lower-ranked monomers, APTES and TEOS (Fig. 2(X), (VIII)) were selected for MIP 2; they demonstrated increased binding capacities and imprinting factors compared to dopamine imprinted MIPs (MIP 1) (Fig. 3). The improved MIP performance can be correlated with the *in silico* analysis, where multi-point binding of the monomers possibly leads to unique polymeric cavities that possess complementary binding sites for strongly capturing the whole protein A. These experimental results along with the computational findings inspired the use of PTES and UPTMS in a 'third' combination (MIP 3). Clearly, these monomers enable maximum multi-point interactions (Table 2) but also introduce new functional groups of phenyl from PTES and urea from UPTMS to generate highly specific binding sites. This effect was confirmed in the exceptional BC (10.5 mg g^{-1}), and the highest imprinting factor of $\sim$5 was obtained for MIP. The relevance of diverse functional groups and multiple-monomer combinations for imprinting can be validated with the contrasting performance of MIP C, which is a control polymer formed only with TEOS serving as both a monomer and cross-linker. In the entire list of monomers, TEOS possesses the minimum functionality that distinctly affects the MIP quality, yielding the lowest BC (*i.e.* 4.8 mg g^{-1}).

These results suggest that unlike the conventional drug design approach, where the ligands are ranked according to their highest binding energy, monomers should be ranked according to the multi-point interactions for effective MIP design. Protein imprinting has rightfully attracted organosilane monomers because they offer functionalities resembling amino acid side chains that bind very effectively to protein residues and directly impact the selectivity and specificity of MIPs.

3.3. Characterization of nanoparticles

To determine the actual size of the synthesized nanoparticles, visualization using HRTEM was performed. As shown in Fig. 4(a)-(i), Fe_3O_4 nanoparticles were spherical with a mean size of $\sim$ 250 nm. In Fig. 4(a)-(ii), MIP has a thin shell of silane polymer coating visible over an iron core. The XRD pattern shown in Fig. 4(b) consists of characteristic peaks (220), (311), (400), (422), (511), and (440), which are in agreement with the inverse cubic spinel phase of Fe_3O_4 (magnetite, JCPDS card no. 85-1436). This confirms that the crystal structure of Fe_3O_4 is preserved in the imprinting performed for Fe_3O_4 nanoparticles, silica-coated Fe_3O_4 nanoparticles, MIP and NIP. In Fig. 4(c)-(i), the peak at 530 cm^{-1} is attributed to Fe–O bond vibration, which is evident to different extents in the spectra of all the given particles. In Fig. 4(c)-(ii), the peak at 1100 cm^{-1} corresponds to Si–O–Si stretching, which confirms the coating of silica on the Fe_3O_4 nanoparticles. Next, in Fig. 4(c)-(iii), the peak at 1630 cm^{-1} represents the stretching vibration of the N–H, indicating the deposition of APTES from the hybrid silane polymer layer. These results suggest the successful functionalization and deposition of the imprinting layer on the magnetic nanoparticles. The presence of surface functional groups after silica coating and imprinting layer were confirmed using FTIR. EDAX analysis was performed to investigate the elemental composition present at various levels of modification. The iron and oxygen peaks in iron oxide nanoparticles are depicted in Fig. 4(d)-(i). Next, after coating with silica, a silicon peak is illustrated in Fig. 4(d)-(ii). A relative increase in the carbon atomic composition was observed in glutaraldehyde-coated nanoparticles (Table S2, ESI†). MIP and NIP nanoparticles showed a comparative increase in silicon atomic composition and a decrease in carbon atomic composition, which can be

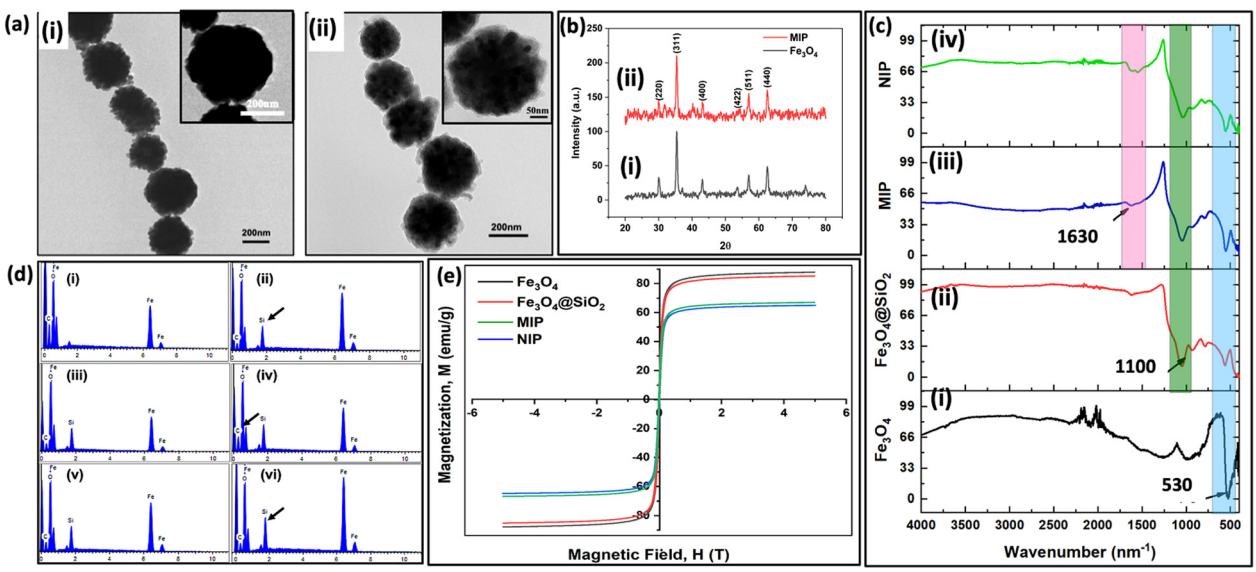

Fig. 4 (a) TEM image of (i) Fe_3O_4 and (ii) MIP in a size range of 250–300 nm; (b) XRD pattern of the (i) Fe_3O_4 and (ii) MIP showing the magnetite nature of nanoparticles. (c) FTIR spectrum at different steps of MIP synthesis, *i.e.*, (i) Fe_3O_4, (ii) Fe_3O_4@SiO_2, (iii) MIP and (iv) NIP; (d) EDX analysis of particles after each step of chemical modification on the surface; (i) iron oxide nanoparticles (MNP), (ii) silica-coated MNP, (iii) APTES-functionalized MNP, (iv) glutaraldehyde-coated MNP, (v) MIP and (vi) NIP; (e) hysteresis loop of Fe_3O_4, Fe_3O_4@SiO_2, MIP and NIP.

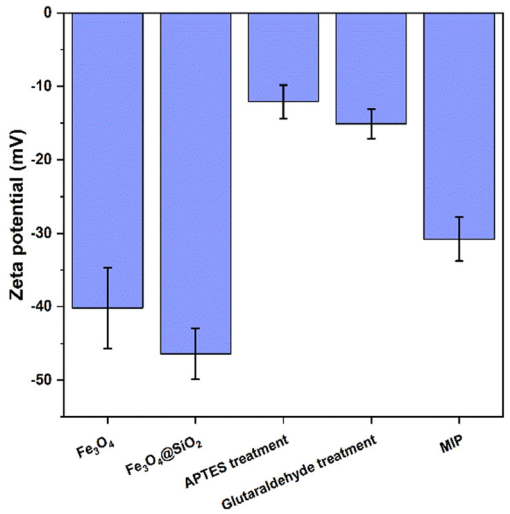

Fig. 5 Zeta-potential for different particles in aqueous media.

attributed to the presence of silane monomers[55] (Fig. 4(d)(v) and (vi)). The magnetic properties of the nanoparticles were measured by the VSM at RT. As shown in Fig. 4(e), the saturation magnetization of Fe_3O_4, Fe_3O_4@SiO_2, MIP, and NIP are 87, 84, 64, and 66 emu g^{-1}, respectively. The decrease in the saturation magnetization is due to the presence of silica coatings over bare MNPs.[56] Despite a reduction in saturation magnetization, the value is sufficient for the efficient separation of MIP in the presence of an external magnetic field. The stability and coating of nanoparticles were determined using Zeta potential values. Zeta potential values obtained for different nanoparticles are depicted in Fig. 5. The surface charge of iron oxide nanoparticles was −40.2, which further decreased to −46.4 due to the presence of added free hydroxyl groups in the silica coating. Next, after coating with APTES, it increased to −12 due to the presence of free amino groups on the surface of the nanoparticles. Then, the reaction with glutaraldehyde decreased the surface charge to −15.1. MIP showed a net negative surface charge (−30.2) due to the polymer layer of the silane monomers. A negative surface charge over the nanoparticle has been shown to facilitate the stability of these particles.[57]

3.4. Protein binding studies

The binding isotherm of protein A binding to MIP and NIP in a concentration range of 0–40 μg mL^{-1} was plotted, as shown in Fig. 6. The adsorption of protein A to MIP is due to the generation of selective binding sites for protein A, indicated by the nearly five-fold lower adsorption on NIP. To further understand the adsorption properties, Langmuir (iii), Freundlich (iv) and Hill (v) equations were applied to fit the experimental results.

$$(C_e/q_e) = (1/(q_{max}K_L)) + (C_e/q_{max}) \quad \text{(iii)}$$

$$\log q_e = (1/n_f)\log C_e + \log K_f, \quad \text{(iv)}$$

$$q_e = q_{max}C_o^n/(C_o^n + K_d^n), \quad \text{(v)}$$

where C_e (μg mL^{-1}) represents the equilibrium concentration of protein A. q_e (μg mg^{-1}) and q_{max} (μg mg^{-1}) are the equilibrium adsorption amount and the maximum adsorption amount, respectively. C_o represents the concentration of protein A added initially. K_L (mL mg^{-1}), K_f (mg g^{-1}) and K_d (mg mL^{-1}) represent the Langmuir, Freundlich and Dissociation constant, respectively. n_f and n are the Freundlich exponent and Hill slope, respectively. The fitting parameters are shown in Table S3 (ESI†). The Hill equation presents a higher correlation coefficient (R^2) than the Langmuir and Freundlich equations; therefore, the Hill equation model fits better in the adsorption study of protein A to MIP. Here, the value of n is 15.63, *i.e.*, more than 1, which indicates cooperativity in binding. The obtained K_d value was 9.33 μg mL^{-1} or 2.2 × 10^{-7} M, which is comparable to the value for actual antibodies (10^{-7} to 10^{-9} M).[58]

To investigate the selectivity of the imprinted polymer, the MIP was incubated with the same concentration of different proteins—BSA, HSA, and Lysozyme. HSA and BSA are 66.5 kDa proteins with a negative net surface charge, similar to protein A. Lysozyme is a 14 kDa protein with a positive net surface charge at physiological pH.

As shown in Fig. 7, protein A showed significantly higher BC with MIP compared to HSA, BSA, and Lysozyme. Although the structures of HSA and BSA are similar, there is an amino acid sequence identity of 76%, leading to few confirmational variations. Therefore, this difference contributes to a change in the binding affinity with MIP. In addition to its high affinity and selectivity with protein A, it is expected that MIP also displays effective binding with whole *S. aureus*.

3.5. Bacterial binding studies

To evaluate the bacterial binding properties of MIP, bacterial concentrations ranging from 10^1 to 10^7 CFU mL^{-1} were used. Fig. 8 shows an increase in bacterial adsorption on MIPs in response to increased bacterial concentrations. Notably, even at the maximum bacterial concentration, surface saturation was not obtained, indicating that the produced MIP surface had sufficient binding capability for the given application.[59] In addition, the magnetic core of the nanoparticles facilitated the *S. aureus* capture and detection at concentrations as low as 10 CFU mL^{-1}.

To study the bacterial selectivity, MIP was incubated with *S. aureus* and other non-specific bacteria, *i.e. B. subtilis, P. aeruginosa and E.coli*. As shown in Fig. 9, *S. aureus* remains bound to MIP even after PBS washing. There was minimum four-fold higher fluorescence in *s. aureus* than other non-specific bacteria, therefore lesser binding in the case of *B. subtilis, P. aeruginosa* and *E. coli.* This study confirms that MIP formed against protein A of *S. aureus* shows specific binding with the target bacteria.

3.6. *S. aureus* detection in real samples

To assess the reliability of the method, the selective isolation of *S. aureus* from cows' milk was conducted, by intentionally spiking it with a known bacterial concentration of 10^6 CFU mL^{-1}.

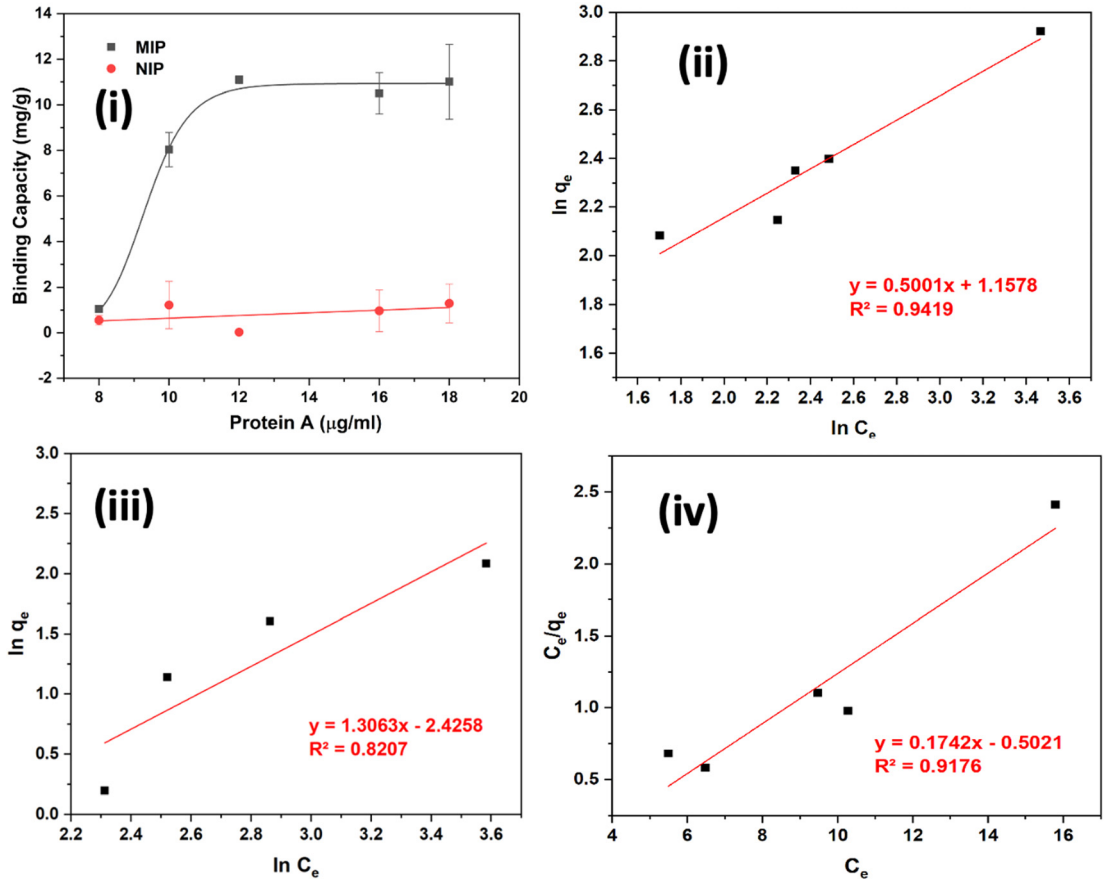

Fig. 6 (i) Amount of protein A (mg) bound per g of MIP and NIP particles against the initial concentration of protein A fitted using the Hill equation. (ii), (iii) Freundlich fitting of MIP and NIP binding isotherm. (iv) Langmuir fitting for MIP binding isotherm.

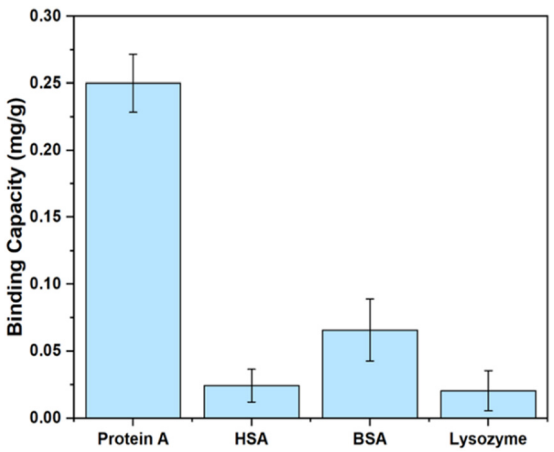

Fig. 7 BC of MIP for protein A and other non-specific proteins, *i.e.*, BSA, HSA and lysozyme. MIP showed 10, 4 and 12-fold better BC for protein A compared to HSA, BSA and lysozyme, respectively.

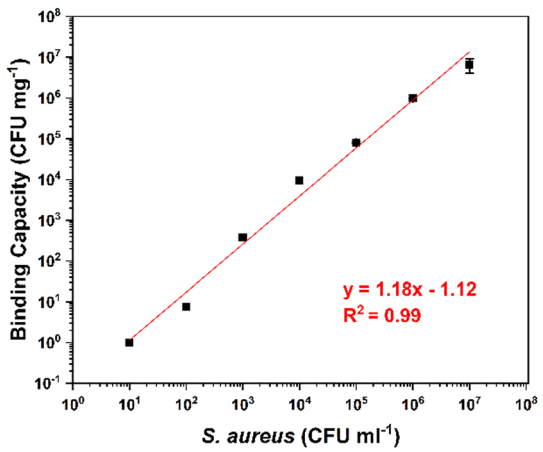

Fig. 8 Adsorption isotherm of *S. aureus* binding to the MIP. Bound *S. aureus* concentration obtained by plating the unbound cells after treatment with MIP (subtraction method).

The choice of milk as the testing medium stems from the potential secretion of *S. aureus* into milk by dairy cows afflicted with mastitis. Table 3 illustrates a notable five-fold increase in BC of MIP compared to NIP. This enhanced binding capability facilitated the specific and efficient detection of *S. aureus* in milk samples. This outcome unequivocally demonstrates that the devised method exhibits robust anti-interference capabilities, enabling the accurate assessment of *S. aureus* concentration in complex mixtures.[59]

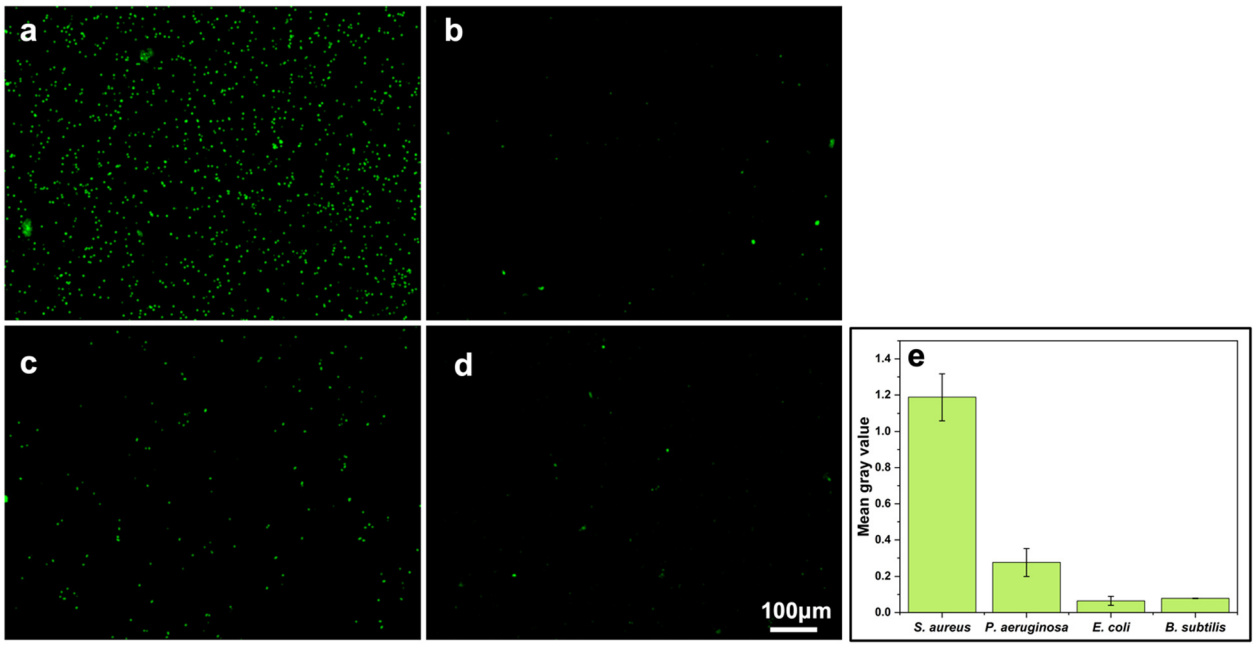

Fig. 9 Fluorescence microscopy images of different bacteria: (a) *S. aureus* (Gram-positive) and (b) *B. subtilis* (Gram positive), (c) *P. aeruginosa* (Gram-negative) (d) *E. coli* (Gram-negative) treated with MIP (0.2 mg ml^{-1}) for 2 h, followed by washing and visualization of MIP bound bacteria. (e) Fluorescence intensity analysis of microscopy images for different bacteria using ImageJ.

Table 3 Comparative binding capacities and cell recovery percentage of molecularly imprinted polymers (MIPs) and non-imprinted polymers (NIPs) presenting selective isolation of *S. aureus* from milk

	S. aureus spiked in milk sample	BC (CFU mg^{-1})	Recovery (%)
MIP	1.26×10^6	1.36×10^6	107.9
NIP	1.26×10^6	2.40×10^5	19.0

4. Conclusions

In this study, we synthesized protein A-imprinted magnetic nanoparticles for biomarker-based *S. aureus* detection. Using *in silico* studies, monomers were rationally selected for the imprinting process based on their interactions with protein A at multiple surface residues and fairly high binding affinity. Comparatively, dopamine showed the highest binding affinity (−4.64 kcal mol^{-1}); however, its limited number of multi-point interactions (4) was reflected in a poor imprinting factor (0.8). In contrast to dopamine, binding at multiple points with non-covalent (reversible) bonds were displayed by silane monomers. MIP 3 displayed a high BC of 11 mg g^{-1} and showed selective binding and capture of protein A as well as *S. aureus* compared to non-specific bacteria, such as *P. aeruginosa*, *E.coli* and *B. subtilis.* In addition, it demonstrated a wide range (10^1 to 10^7 CFU mL^{-1}) of *S. aureus* capture and detection as well as ~100% recovery of *S. aureus* (10^6 CFU mL^{-1}) from spiked milk samples. Instead of antibodies,[60,61] cost effective, stable and selective MIPs may be employed as sensing elements capable of direct integration in different *in vitro* diagnostic devices.[62] Similar to antigen–antibody interactions, this study clearly demonstrates the importance of multipoint interactions of monomers in the rational design of MIPs.[63,64] Intervention with predictive computational modelling results in high-performing MIPs, thus reducing the need for extensive experimental design. This can accelerate the process of point-of-care device development and application, especially in resource-constrained developing nations. Biomarker imprinted bacterial detection can be applied to other ESKAPE pathogens for simultaneous detection in a multiplex platform, therefore taking a step further for the rapid detection and treatment of bacterial infections. It has further applications in the detection of food contamination, pathogen outbreaks and other infections.

Author contributions

The manuscript was prepared with the involvement of all the authors. All authors have approved the manuscript's final version.

Conflicts of interest

The authors declare no conflict of interest.

Acknowledgements

The project was financially supported by DST/NM/NNetRA/2018(G)-IITD from Department of Science and Technology (DST) and 5(1) 2017-NANO from Ministry of Electronics and Information Technology (MeitY), Govt. of India. The authors acknowledge Central Research Facilities (CRF) and Nanoscale

Research Facilities (NRF) at IITD for the instrumentation facilities. SB and SK express gratitude to Ministry of Human Resource Development (MHRD), Govt. of India, for Institute postdoctoral fellowship, IIT Delhi. KN would like to thank the MHRD for the research fellowship.

References

1 S. Y. C. Tong, J. S. Davis, E. Eichenberger, T. L. Holland and V. G. Fowler, *Clin. Microbiol. Rev.*, 2015, **28**, 603–661.
2 F. Der Wang, Y. Y. Chen, T. L. Chen and C. Y. Liu, *Am. J. Infect. Control*, 2008, **36**, 118–122.
3 F. Alonzo and V. J. Torres, *Microbiol. Mol. Biol. Rev.*, 2014, **78**, 199–230.
4 A. F. Haag, J. R. Fitzgerald and J. R. Penadés, *Microbiol. Spectrum*, 2019, **7**, 10–1128.
5 N. Wellinghausen, A. J. Kochem, C. Disqué, H. Mühl, S. Gebert, J. Winter, J. Matten and S. G. Sakka, *J. Clin. Microbiol.*, 2009, **47**, 2759–2765.
6 D. J. Speers, T. R. Olma and G. L. Gilbert, *J. Clin. Microbiol.*, 1998, **36**, 1032–1034.
7 B. S. Reisner and G. L. Woods, *J. Clin. Microbiol.*, 1999, **37**, 2024–2026.
8 A. Nouri, H. Ahari and D. Shahbazzadeh, *Int. J. Biol. Macromol.*, 2018, **107**, 1732–1737.
9 O. G. Brakstad, K. Aasbakk and J. A. Maeland2, *J. Clin. Microbiol.*, 1992, **30**, 1654–1660.
10 K. T. Lim, C. S. J. Teh and K. L. Thong, *Biomed. Res. Int.*, 2013, 895816.
11 W. Kong, J. Xiong, H. Yue and Z. Fu, *Anal. Chem.*, 2015, **87**, 9864–9868.
12 N. Ghanwate, P. Thakare, P. R. Bhise and S. Gawande, *Sci. Rep.*, 2016, **6**, 1–5.
13 J. J. Belbruno, *Chem. Rev.*, 2019, **119**, 94–119.
14 P. Mishra, K. Griebenow and A. M. Klibanov, *Biotechnol. Bioeng.*, 1996, **52**, 609–614.
15 J. Pan, X. Xue, J. Wang, H. Xie and Z. Wu, *Polymer*, 2009, **50**, 2365–2372.
16 X. Xue, J. Pan, H. Xie, J. Wang and S. Zhang, *React. Funct. Polym.*, 2009, **69**, 159–164.
17 Y. Guo, J. Li, X. Song, K. Xu, J. Wang and C. Zhao, *ACS Appl. Bio Mater.*, 2021, **4**, 420–427.
18 J. Bezdekova, K. Zemankova, J. Hutarova, S. Kociova, K. Smerkova, V. Adam and M. Vaculovicova, *Food Chem.*, 2020, **321**, 126673.
19 A. Aherne, C. Alexander, M. J. Payne, N. Perez and E. N. Vulfson, *J. Am. Chem. Soc.*, 1996, **118**, 8771–8772.
20 J. Borovička, S. D. Stoyanov and V. N. Paunov, *Nanoscale*, 2013, **5**, 8560–8568.
21 X. Shen, J. Svensson Bonde, T. Kamra, L. Bülow, J. C. Leo, D. Linke and L. Ye, *Angew. Chem., Int. Ed.*, 2014, **53**, 10687–10690.
22 G. Ertürk, D. Berillo, M. Hedström and B. Mattiasson, *Biotechnol. Rep.*, 2014, **3**, 65–72.
23 M. Marc, *Mip Synthesis, Characteristics and Analytical Application*, Elsevier, 2019.
24 J. Liu, Q. Deng, D. Tao, K. Yang, L. Zhang, Z. Liang and Y. Zhang, *Sci. Rep.*, 2014, **4**, 1–6.
25 T. Cowen, K. Karim and S. Piletsky, *Anal. Chim. Acta*, 2016, **936**, 62–74.
26 R. Borozniak, J. Reut, A. Tretjakov, A. Lomaka, A. Öpik and V. Syritski, *J. Mol. Recognit.*, 2017, **30**, 2635.
27 S. Suryana, Mutakin, Y. Rosandi and A. N. Hasanah, *Molecules*, 2021, **26**, 1891.
28 M. v Sullivan, S. R. Dennison, G. Archontis, S. M. Reddy and J. M. Hayes, *J. Phys. Chem. B*, 2019, **123**, 5432–5443.
29 D. R. Kryscio, Y. Shi, P. Ren and N. A. Peppas, *Ind. Eng. Chem. Res.*, 2011, **50**, 13877–13884.
30 S. Rajpal, S. Singh, P. Mishra and S. Bhakta, *Molecularly Imprinted Polymers (MIPs): Commercialization Prospects, Meenakshi Singh*, Elsevier, vol. 16, pp. 391–415.
31 M. K. Sandel and J. L. McKillip, *Food Control*, 2004, **15**, 5–10.
32 H. Deng, X. Li, Q. Peng, X. Wang, J. Chen and Y. Li, *Angew. Chem., Int. Ed.*, 2005, **44**, 2782–2785.
33 A. Saha, K. Narula, P. Mishra, G. Biswas and S. Bhakta, *Nanoscale Adv.*, 2023, **5**, 1386–1396.
34 A. H. Lu, E. L. Salabas and F. Schüth, *Angew. Chem., Int. Ed.*, 2007, **46**, 1222–1244.
35 B. T. Thanh, N. van Sau, H. Ju, M. J. K. Bashir, H. K. Jun, T. B. Phan, Q. M. Ngo, N. Q. Tran, T. H. Hai, P. van Hung and T. T. Nguyen, *J. Nanomater.*, 2019, 2182471.
36 F. Chen, M. Mao, J. Wang, J. Liu and F. Li, *Talanta*, 2020, **209**, 120509.
37 S. Bhakta, M. S. I. Seraji, S. L. Suib and J. F. Rusling, *ACS Appl. Mater. Interfaces*, 2015, **7**, 28197–28206.
38 E. F. Pettersen, T. D. Goddard, C. C. Huang, G. S. Couch, D. M. Greenblatt, E. C. Meng and T. E. Ferrin, *J. Comput. Chem.*, 2004, **25**, 1605–1612.
39 G. M. Morris, R. Huey, W. Lindstrom, M. F. Sanner, R. K. Belew, D. S. Goodsell and A. J. Olson, *J. Comput. Chem.*, 2009, **30**, 2785–2791.
40 A. A. Lahcen, S. G. Surya, T. Beduk, M. T. Vijjapu, A. Lamaoui, C. Durmus, S. Timur, O. Shekhah, V. Mani, A. Amine, M. Eddaoudi and K. N. Salama, *ACS Appl. Mater. Interfaces*, 2022, **14**, 49399–49424.
41 C. Lafarge, M. Bitar, L. El Hosry, P. Cayot and E. Bou-Maroun, *Mater. Today Commun.*, 2020, **24**, 101157.
42 G. Goyal, S. Bhakta and P. Mishra, *ACS Appl. Nano Mater.*, 2019, **2**, 6747–6756.
43 M. M. Bradford, *Anal. Biochem.*, 1976, **72**, 248–254.
44 W. Zhang, X. She, L. Wang, H. Fan, Q. Zhou, X. Huang and J. Z. Tang, *Materials*, 2017, **10**, 475.
45 J. Chen, S. Lei, Y. Xie, M. Wang, J. Yang and X. Ge, *ACS Appl. Mater. Interfaces*, 2015, **7**, 28606–28615.
46 N. Idil, M. Bakhshpour, I. Perçin and B. Mattiasson, *Biosensors*, 2021, **11**, 140.
47 Peptide calculator, **https://www.bachem.com/knowledge-center/peptide-calculator/**, (accessed 30 October 2022).
48 J. J. Lee, K. J. Jeong, M. Hashimoto, A. H. Kwon, A. Rwei, S. A. Shankarappa, J. H. Tsui and D. S. Kohane, *Nano Lett.*, 2014, **14**, 1–5.

49 A. Lamaoui, A. A. Lahcen and A. Amine, *Polymers*, 2023, **15**, 3712.
50 W. Li, Q. Zhang, Y. Wang, Y. Ma, Z. Guo and Z. Liu, *Anal. Chem.*, 2019, **91**, 4831–4837.
51 Z. Guo, R. Xing, M. Zhao, Y. Li, H. Lu and Z. Liu, *Adv. Sci.*, 2021, **8**, 2101713.
52 W. Li, Q. Zhang, Y. Wang, Y. Ma, Z. Guo and Z. Liu, *Anal. Chem.*, 2019, **91**, 4831–4837.
53 R. Xing, Z. Guo, H. Lu, Q. Zhang and Z. Liu, *Sci. Bull.*, 2022, **67**, 278–287.
54 R. Gao, X. Kong, X. Wang, X. He, L. Chen and Y. Zhang, *J. Mater. Chem.*, 2011, **21**, 17863–17871.
55 S. Rajpal, S. Bhakta and P. Mishra, *J. Mater. Chem. B*, 2021, **9**, 2436–2446.
56 L. Liu, X. Zhu, Y. Zeng, H. Wang, Y. Lu, J. Zhang, Z. Yin, Z. Chen, Y. Yang and L. Li, *Polymers*, 2018, **10**, 1329.
57 S. Bhattacharjee, *J. Controlled Release*, 2016, **235**, 337–351.
58 X. Bi and Z. Liu, *Anal. Chem.*, 2014, **86**, 959–966.
59 J. Bezdekova, K. Zemankova, J. Hutarova, S. Kociova, K. Smerkova, V. Adam and M. Vaculovicova, *Food Chem.*, 2020, **321**, 126673.
60 S. Joseph, S. Rajpal, D. Kar, S. Devinder, S. Pandey, P. Mishra and J. Joseph, *Biosens. Bioelectron.*, 2023, **241**, 115695.
61 S. Sharma, D. Kar, A. Moudgil, S. Das and P. Mishra, *Sens. Actuators, B*, 2024, **407**, 135486.
62 S. Rajpal and P. Mishra, *Biosens. Bioelectron.: X*, 2022, **11**, 100201.
63 S. Rajpal, B. Mizaikoff and P. Mishra, *Int. J. Biol. Macromol.*, 2024, **266**, 131101.
64 S. Rajpal, P. Mishra and B. Mizaikoff, *Int. J. Mol. Sci.*, 2023, **24**, 6785.